

# Simulations of the lower-hybrid antenna in the Madison Symmetric Torus reversed-field pinch

Johan Carlsson<sup>1</sup>‡, Michael Kaufman<sup>2</sup>§, John Goetz<sup>2</sup>, David Smithe<sup>1</sup> and Mark Thomas<sup>2</sup>

<sup>1</sup>Tech-X Corporation, 5621 Arapahoe Avenue, Boulder, Colorado, USA

<sup>2</sup>Department of Physics, University of Wisconsin–Madison, USA

E-mail: carlsson@pppl.gov

**Abstract.** Due to constraints inherent to a reversed-field pinch plasma configuration, an unusual launch structure – the interdigital line – was used for lower-hybrid current-drive experiments in the Madison Symmetric Torus. The antenna design and performance were analyzed using an array of codes (including RANT3D/AORSA1D-H, Microwave Studio and VORPAL). It was found that the voltage phasing was not the intended one. As a result, the parallel-wavenumber spectrum of the launched wave peaks at a value lower than desired, making the accessibility marginal. Further simulations demonstrated that the error can largely be corrected by either lowering the antenna operating frequency or shortening the length of the resonators.

## 1. Introduction

Uchimoto *et al.* used ray tracing and MHD simulation with an ad hoc force term to show that edge lower-hybrid (LH) poloidal current drive could suppress tearing-mode activity in Reversed-Field Pinches (RFPs) in order to improve confinement [1]. For optimal effect, it was shown that the driven current should peak just inside the reversal surface, which is at about 0.8 of the minor radius and where the toroidal magnetic field changes sign. For the Madison Symmetric Torus (MST) [2] it was estimated that at least 1 MW of absorbed power would be necessary.

Recently, a proof-of-concept experimental effort was made at MST to gradually start testing Uchimoto’s scheme *in situ* [3]. This paper is about the simulations done in support of this effort.

RF sources at 800 MHz were available free of cost and this frequency was therefore chosen. At 800 MHz, the fast wave would in MST have to tunnel about 5 cm from an antenna into the plasma to propagate, an unacceptably long distance. Launching a slow wave is the more feasible option for current drive in MST. The slow wave starts propagating much closer to the plasma edge and with a short enough parallel wavelength

‡ Present institution: Crow Radio and Plasma Science

§ Present institution: Oak Ridge National Laboratory

it could in principle propagate all the way to the lower-hybrid resonance deep inside the plasma. The primary constraint on a launch structure is then that it excites a wave with

$$n_{\parallel} = \frac{c k_{\parallel}}{\omega} > 7.5, \quad (1)$$

to avoid cut off inside the plasma. Unfortunately it would not be possible to use the standard LH grill antenna in MST because the large porthole it would require to fit through the conducting shell would introduce large field errors and destroy MHD stability. The conducting shell must not only be free of large portholes, it must also be close fitting to the plasma. A launch structure inside the conducting shell would have to be very flat, less than 2 cm in the radial direction on the inboard side and even less on the outboard side. The largest porthole in MST is 11.43 cm in diameter and it would be highly desirable if the launch structure could be installed through this porthole. With these severe constraints, an unusual design was chosen: the interdigital line.

### 1.1. The MST LH antenna

The interdigital line traveling-wave antenna design, chosen to meet the difficult requirements discussed in the previous section, is based on the interdigital bandpass filter proposed by Matthaei [4]. It is similar to combline [5, 6] and fishbone [7] antennas, even though those are both operated at much lower frequencies for fast-wave launch. Like the combline antenna, the interdigital line has a set of parallel resonators that are capacitively and/or inductively coupled to propagate a wave down the structure. Unlike the combline, which has resonators all grounded on the same side and open on the opposite side, the interdigital line has resonators that are alternately grounded on opposite sides. In fact, the interdigital line can be thought of as two interleaved comblines. The MST implementation of the interdigital line [3] has grounded planes both at the back and the front of the antenna, with an aperture in the front plane. According to approximate analytic theory, the phase difference between resonator rods is determined solely by the length of the rods. However, as we shall discuss later, in this respect this theory is simplistic. The theory does correctly predict that the voltage and current phasings differ by  $180^{\circ}$ . The interdigital line will thus launch two counter-propagating waves, one voltage (electric) wave and one current (magnetic) wave, which might, on a side note, qualify it as a meta material. To suppress competition between the counter-propagating waves, it is desirable for the launch structure to have a large impedance to minimize the amplitude of the current wave. For the latest version (MkIII) of the MST interdigital line, CST Microwave Studio<sup>®</sup> was used to fine tune the design and computed the self-impedance of the rods (rod-to-ground plane) to be about  $100 \Omega$  and the mutual impedance (rod-to-rod) to be about  $3000 \Omega$ .

Another attractive feature of the interdigital line is that it can be powered by thin coaxial feeds. The MkIII antenna uses  $1\frac{5}{8}$ " coax feeds fitting through 2" port holes. For impedance matching between the  $50 \Omega$  coax and the  $100 \Omega$  antenna, three matching straps are used.

For a thorough discussion of the MST interdigital line we refer to Chapter 2.1 of Ref. [8].

## 2. Simulations

A small arsenal of codes was used to analyze the MkIII MST LH antenna, including RANT3D/AORSA1D-H [9], CST Microwave Studio<sup>®</sup> (MWS), VORPAL<sup>®</sup> [10] and COMSOL Multiphysics<sup>®</sup> [11]. COMSOL was only used late in the project and its results were deemed less reliable than earlier VORPAL results and will therefore not be presented here, but can be found in Chapter 2.2 of Ref. [8]. The MkI antenna was designed simply using the approximate analytic theory of Matthaei [4] and SPICE circuit simulation to model the coupled transmission lines and fine-tune the phasing given a fixed geometry. The MkII was designed additionally using FastCap (3D electrostatic finite-element method) to accurately compute the rod end capacitances, neglected for MkI. Only for designing the impedance matching straps of the MkIII version was MWS finally brought in. All the codes used a flattened model of the antenna, except VORPAL, which used a fully realistic model, as shown in Fig. 4.

The plasma parameters used for all the simulations presented here are those of a standard MST discharge with 400 kA of plasma current. LH experiments have also been performed for higher-confinement pulsed poloidal current drive discharges with gas puffing used to compensate for the decrease in edge plasma density, but these are beyond the scope of this paper. For a standard discharge the distance from the antenna to the plasma edge is 1.3 cm.

### 2.1. RANT3D/AORSA1D-H simulations

RANT3D solves for the electromagnetic fields in and around an antenna, where the antenna is modeled as a set of conductors with prescribed currents. Following Golant's RF coupling theory [12], the plasma is described by an impedance matrix at the assumed vacuum-plasma interface. The version of RANT3D we used loads an impedance matrix computed by the AORSA1D-H code. AORSA1D-H is a tokamak code and several modifications were necessary to make it work for a Reversed-Field Pinch (RFP), such as the MST. Perhaps the most important one was to include the poloidal upshift of the parallel wave number. In an RFP the edge magnetic field is predominantly in the poloidal direction and the parallel wave number is therefore roughly equal to  $m/r$  where  $m$  is the poloidal mode number and  $r$  is the minor radius. As a wave propagates into the plasma,  $m$  remains fixed but  $r$  decreases and the parallel wave number increases (is upshifted). The upshift is critical to avoid reflection and also increases the Landau damping, as shown in Fig. 1.

The Fourier transform of the Poynting flux is shown in Fig. 2. The  $n_{\parallel}$  ( $n_z$  in the plots) peaks at 7.5, right where Matthaei's theory predicts the contribution from the dominant voltage wave to be, determined by rod length and rod-to-rod separation. The

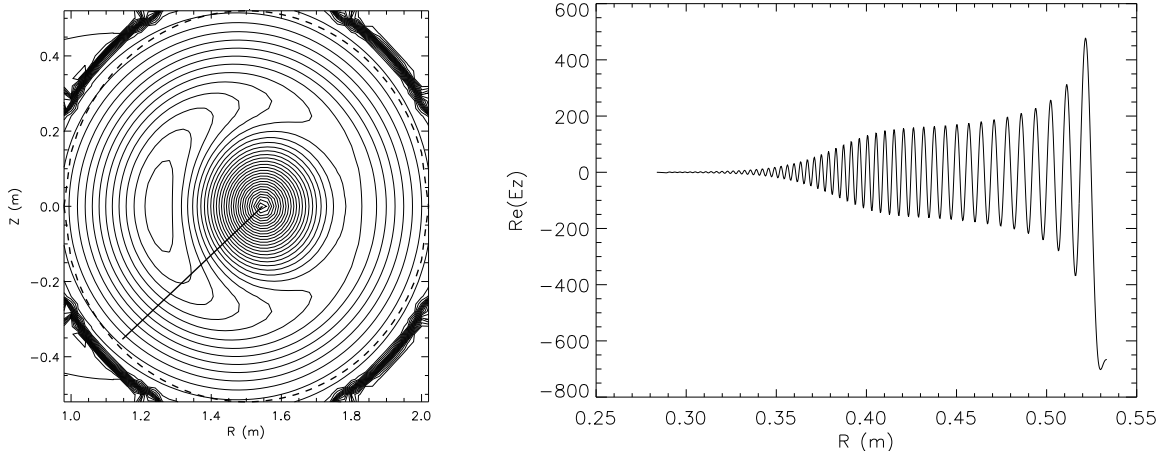


**Figure 1.** Left: Contour plot of poloidal magnetic field from an MSTFIT equilibrium with the thick diagonal line showing the one-dimensional simulation domain of AORSA1D-H. Right:  $\Re E_z$  as function of minor radius. Wave is launched from antenna with  $n_{\parallel} = 7.5$ . When it reaches  $r = 0.38$  m it is upshifted to  $n_{\parallel} \approx 10.5$ , causing very strong electron Landau damping.

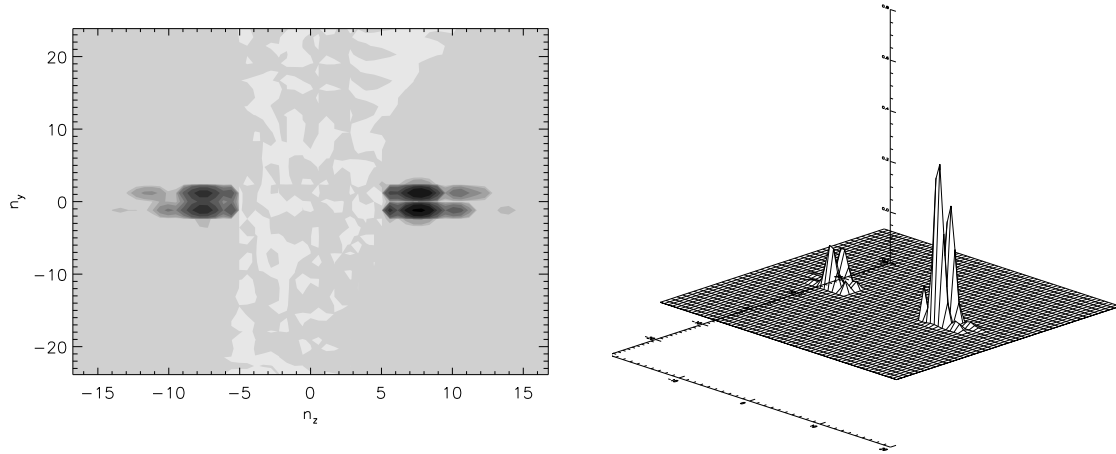


**Figure 2.** Plots of  $\Re P_x$  (real part of radial Poynting flux) in wave number space. Contour plot to the left, darker here means more power entering the plasma. Surface plot to the right.

secondary peak at  $-7.5$  comes from a superposition of reflected voltage wave (due to imperfect impedance matching) and the launched current wave, which, as mentioned above, is phased oppositely of the electric wave for an interdigital line antenna. The peaking of  $n_{\perp}$  ( $n_y$  in the plots) at  $\pm 1$  is also explained by theory, which describes the wave travelling along a resonator rod (in the  $y$ -direction) as a quasi-TEM mode. The  $n_{\perp} = +1$  peak comes from the rods grounded on one side of the antenna and the  $n_{\perp} = -1$  from the rods grounded on the opposite side.

The radial Poynting flux is given by

$$P_x = \frac{1}{2\mu_0}(E_y B_z^* - E_z B_y^*).$$

The plasma load is defined as

$$Z = 2 \frac{\int_z \int_y P_x dy dz}{\sum_{k=1}^{16} I_k I_k^*},$$

where the digits are numbered from  $k = 1$  to  $k = 16$  and  $I_k$  is the RMS current on digit  $k$ . In the RANT3D simulations this load is computed to be  $3.2 \Omega$ , with 11 W of power entering the plasma and the sum of currents squared  $6.6 \text{ A}^2$  (1 A on the first digit). This should be considered an acceptable load for the relatively high frequency. As usual, the load depends sensitively on antenna-plasma distance. In the simulations, reducing the antenna-plasma distance by a mere 3 mm (to 1.0 cm) more than doubles the plasma load to  $6.8 \Omega$ . Increasing the distance by 3 mm (to 1.6 cm) decreases to load to  $2.2 \Omega$ .

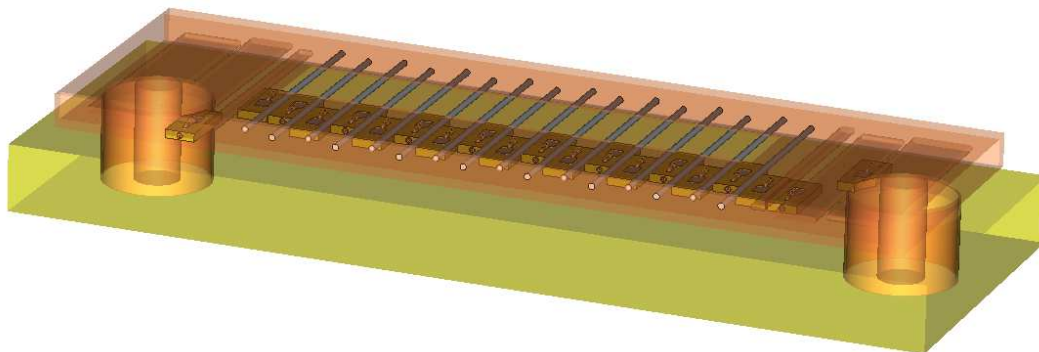
Under the assumption of  $+90^\circ$  voltage phase difference between adjacent antenna rods, the MST LH antenna should thus work well. However, as we will find below, the actual voltage phase difference is smaller than that.

## 2.2. MWS simulations

MWS is a general-purpose electromagnetic solver that uses the Finite Integration Technique, which solves the integral form of Maxwell's equations. The solver numerically solves the equations within a finite domain and can use multiple grid shapes, though for these simulations, a hexahedral mesh is used. Depending on the problem type, either transient, frequency domain, or eigenmode solvers can be used. Since we are interested in the antenna's bandpass characteristics and the transient solver returns the behavior over a broad frequency range with little time penalty and allows open boundary conditions, we use the transient solver.

To monitor the voltages and fields on the antenna a set of virtual diagnostics are used. The components of the electric and magnetic fields can be measured at a specific coordinate, or the entire vector field at a specific frequency can be measured. A voltage can be found by integrating along a prescribed path: in our case, the voltages of interest include between neighboring resonators as well as between a resonator and the antenna backplane. While current probes were not supported at the time of the modeling, a magnetic field probe acted as a proxy for a current phase diagnostic.

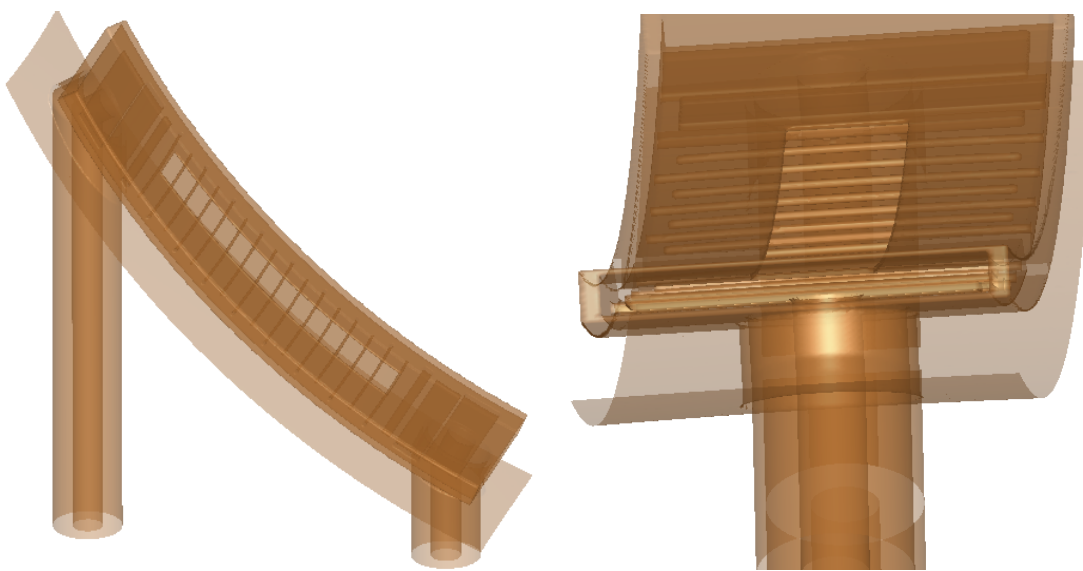
To optimize the impedance matching sections of the antenna, a flattened version of the MkIII antenna was sufficient, and that model is used here. A flat model has the advantages of being much simpler to (virtually) instrument, characterize, and mesh. For a given mesh density, a flat model simulation run takes approximately a quarter of the time. The model used is shown in Figure 3. For a plasma, use of the MWS anisotropic dielectric model was attempted, but not successfully. The results here are for vacuum with open boundary conditions.



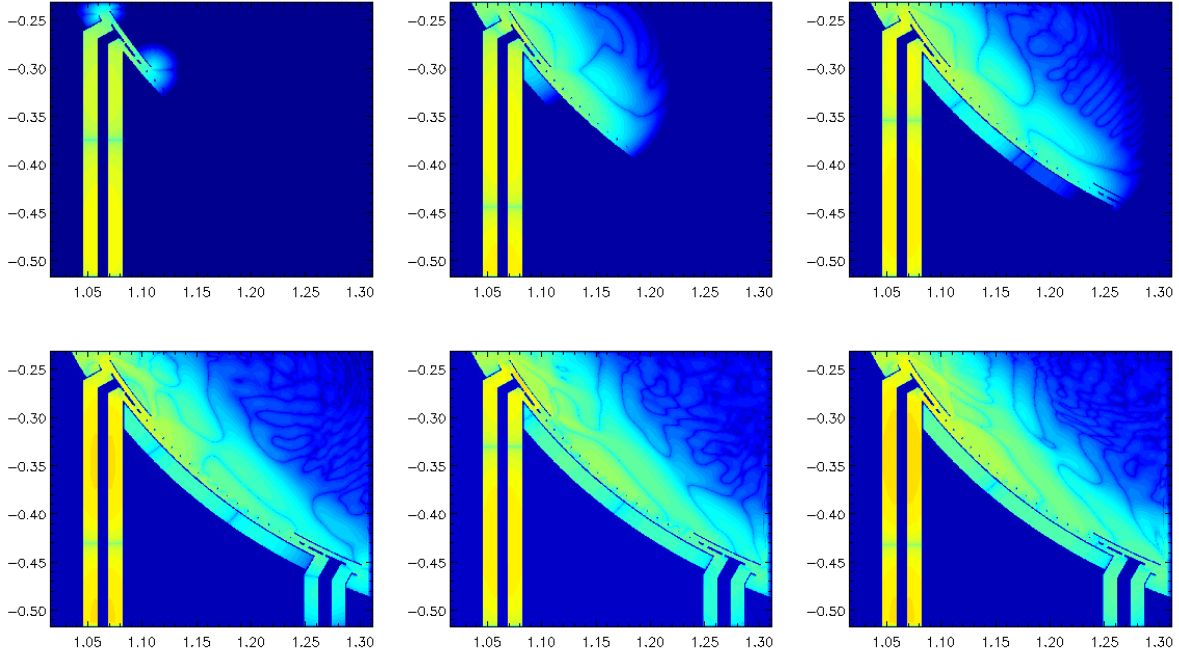
**Figure 3.** MWS flat model of the MkIII antenna.

### 2.3. VORPAL simulations

As mentioned above, the VORPAL simulations were the only ones that utilized a realistic, curved antenna geometry and a plasma model to load the antenna. The antenna model was not loaded from a CAD file, but rather hand coded as a macro in the input file. The antenna model used by VORPAL is shown in Fig. 4. VORPAL is primarily a Particle-In-Cell (PIC) code, but has a variety of other models for reduced particle dynamics. For the simulations of the MST LH antenna we used the standard explicit Yee update for the electromagnetic field and a cold-plasma time-domain dielectric for the electrons [13]. The cold electrons are sufficient to simulate the propagation of the launched slow wave, but obviously not the primary absorption



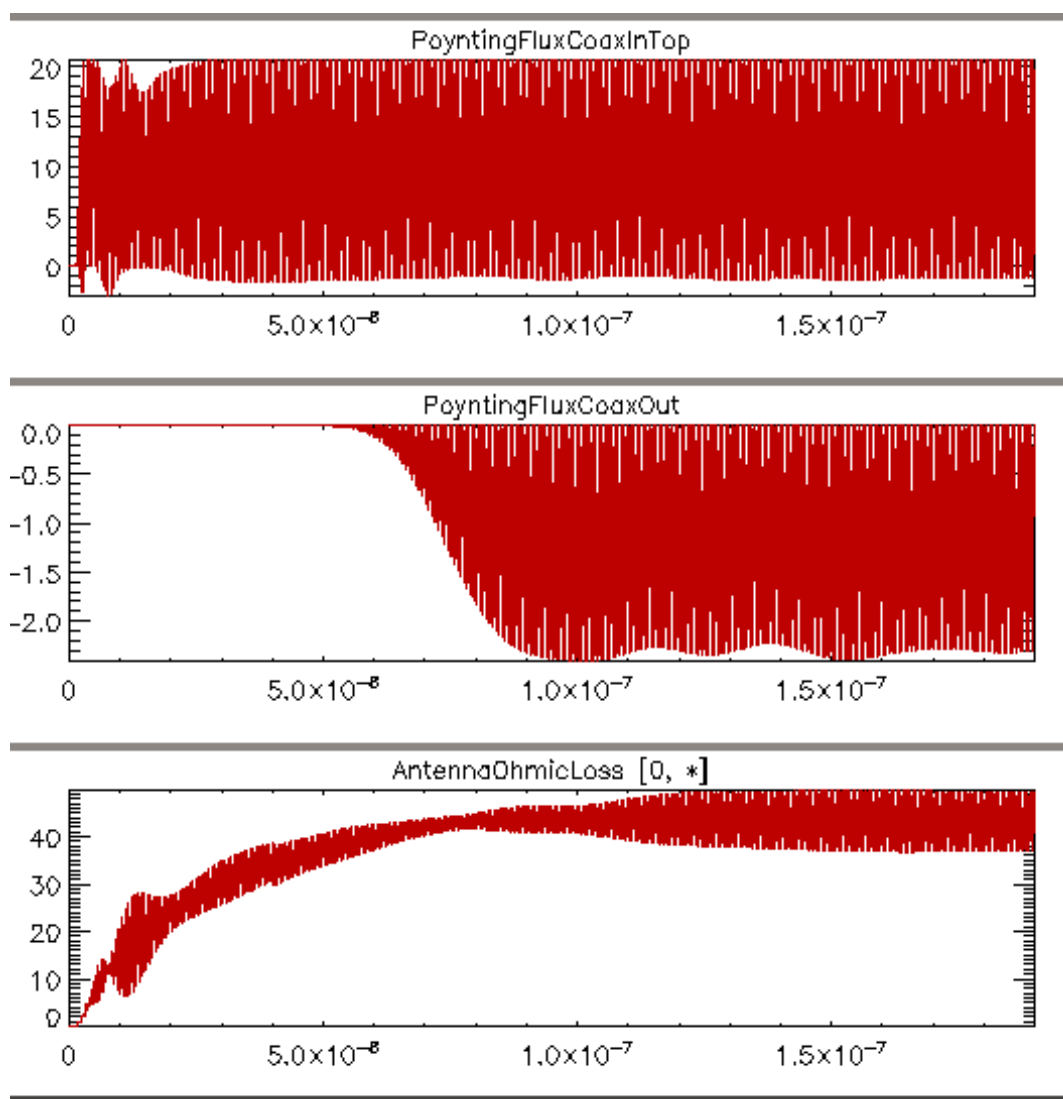
**Figure 4.** Model of MST LH antenna (including co-axial power feeds and part of vacuum vessel) used in VORPAL. Artificial transparency added to show interior detail. Whole antenna to the left and close up to the right.



**Figure 5.** Electric-field component  $E_x$  a quarter RF cycle apart (at times  $ft = 3/4, 4/4, 5/4, 6/4, 7/4, 8/4$ ) after power was turned on. Plot of the plane  $z = 0$ , with  $x$  on the abscissa and  $y$  on the ordinate. The 16 antenna rods are visible as a diagonal of blue dots, indicating zero electric field in the conducting rods.

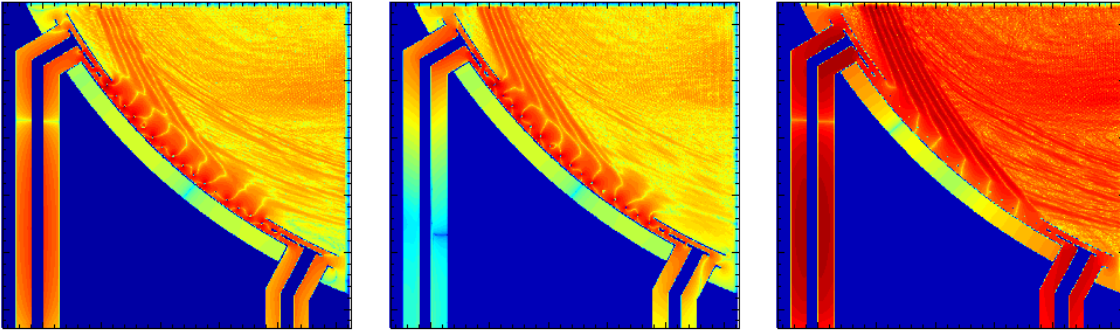
mechanism, electron Landau damping. In the simulations the slow wave is therefore only collisionally absorbed with whatever remaining Poynting flux reaching the edges of the simulation domain 100% absorbed by a numerical Perfectly Matched Layer (PML) [14]. VORPAL uses finite differences for spatial discretization, i.e. the spatial grid is not aligned with the curved conducting surfaces of the antenna. To allow the conducting surfaces to cut through cells in the spatial grid, the Dey-Mittra algorithm [15] was used. The ability to handle curved surfaces well was critical for the decision to use VORPAL as an antenna modeling code. On the other hand, VORPAL is a time-domain code and the reduced electron model used required use of an explicit time step, which imposes a severe CFL condition. The decision was nevertheless made to accept the inefficiencies of having to use several thousand time steps per RF cycle. A typical simulation would use several hundred thousand time steps, sometimes even a million or two, and run for one or several months on a dedicated 34-processor cluster. The need to resolve both the rod width and the small gap between the rod tips and the antenna side wall demanded a sub-millimeter cell size and led to a memory requirement of tens of gigabytes of RAM for the whole simulation domain. Several terabytes of simulation data were generated throughout the project.

Fig. 5 shows the antenna being lit up by the EM field during the first two RF cycles after the power is turned on. The field was excited by a current source at the



**Figure 6.** Cropped screen dump from VorpelView, the primary visualization tool used by this project. The abscissa is the time from when the power is turned on and for the next 150 RF cycles (in seconds). The unit of the Poynting fluxes is  $W/m^2$ . The unit of the ohmic loss is  $W/\Omega$  and if it's multiplied by the sheet resistance (resistivity divided by skin depth) of the antenna material one gets the ohmic loss in  $W$ . For copper at 800 MHz we calculated the sheet resistance to be  $7.4m\Omega$ .

bottom of the coax. The simulations were run until well after the transients died down for the Poynting flux out the lower coax, typically one, or a few, hundred RF cycles. An example is showed in Fig. 6, where two local and one global quantity are plotted against time. The local quantities are the Poynting fluxes entering and exiting the coax feeds of the launch structure, respectively. The global quantity is the ohmic power loss over the whole launch structure. The plots of Fig. 6 show that the simulation had reached approximate steady state when it ended.



**Figure 7.** Magnetic-field components  $B_x$ ,  $B_y$  and  $B_z$  (left to right) after 150 RF cycles with power input into the left-hand coaxial feed.

### 3. Results

The VORPAL<sup>®</sup> simulations showed that the MST interdigital line LH antenna does launch a wave into the plasma, see Fig. 7. The primary (voltage) wave is launched north-northwest with a faint secondary counter-propagating wave launched east-southeast. This secondary wave is likely due to a small reflection off the almost-but-not-quite-matched impedance-matching section on the output side of the antenna, possibly also with some contribution from the current wave. Note how efficiently the PML boundaries soak up the wave energy in the region within a few cells of the domain boundary.

The VORPAL simulations also showed that the current phasing between adjacent rods was about  $-105^\circ$  [16] (giving a voltage phasing of  $+75^\circ$ ), well off from the intended  $-90^\circ$ . This discrepancy was surprisingly large and to build confidence in the VORPAL results, a blind validation exercise was done. MWS had previously been used to analyze the antenna, but difficulties had been encountered when using its anisotropic dielectric to model the plasma. The comparison was therefore done for the vacuum case, where VORPAL gave a voltage phasing of  $+81.2^\circ$ . It was then revealed that the benchmark experimentally measured phasing was  $+79.8^\circ$ , with VORPAL thus just over one degree off. The MWS result was  $+77.1^\circ$ , a couple of degrees off with the simplified, flattened antenna model and with the curved antenna model performing considerably worse. These results are shown in Fig. 8a. It was concluded that the VORPAL simulations were accurate, with an error bar for the voltage and current phasings of roughly one degree.

When the antenna design was revisited, it was discovered that effect of the aperture, visible in Fig. 4, on the antenna impedance, and thus on the voltage and current phasings, was not considered. The incorrect phasing will increase the parallel wave length of the launched electric wave and result in  $n_{\parallel} \approx 6.4$ , a bit low for good accessibility. The focus of the VORPAL and MWS simulations therefore shifted from analyzing the existing MkIII antenna (we will refer to these as Case A simulations below) to finding the optimal way to redesign the antenna. Since the aperture cannot be removed, two

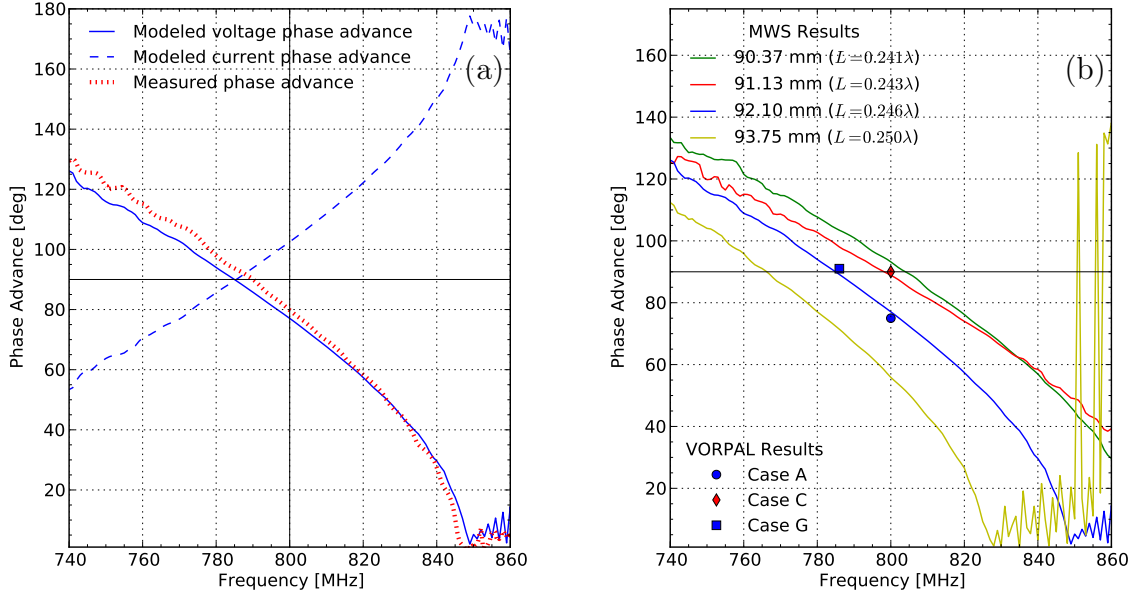


**Figure 8.** Phase advance of flat antenna model as a function of frequency in the passband. Solid lines are the phase advance of the voltage between each resonator and grounded backplane. The dashed line is the phase advance of the current on each resonator. a) The antenna with resonators at the designed 92.1 mm ( $0.246\lambda$ ) in length. The dotted line is the phase advance of the power in vacuum as measured by the loop diagnostics in the backplane of the constructed antenna. b) The antenna with resonators of different lengths with respect to the vacuum wavelength. VORPAL results for Cases A, C, G are shown as well.

alternative approaches were taken to the redesign. In Case C the length of the antenna rods was shortened by 1.3 mm and in Case G the frequency was lowered by 14 MHz. The latter would be preferable as it is easier to retune the transmitter with the as-built antenna rather than building a new antenna.

The simulation results are summarized in Table 1 and Fig. 8b. As can be seen, both redesigns (Cases C and G) corrected the voltage phasing, giving close to the desired  $+90^\circ$ . However, the fraction of power injected into the launch structure that is radiated into the plasma ( $P_{rad}/P_{inj}$ ) is about 10% lower for Cases C and G than for Case A, despite the excellent plasma load of  $9.9 \Omega$  for Case C.

Case	Frequency	Rod length	Phasing	$P_{rad}/P_{inj}$	$P_{\Omega}/P_{inj}$	Plasma load
A	800 MHz	92.1 mm	$+75^\circ$	87%	3.3%	$4.4 \Omega$
C	800 MHz	90.8 mm	$+90^\circ$	77%	4.7%	$9.9 \Omega$
G	786 MHz	92.1 mm	$+91^\circ$	76%	4.2%	$3.6 \Omega$

**Table 1.** Parameters and figures of merit for the antenna configurations considered.

#### 4. Discussion and conclusion

Our simulation work supports the idea that LH should be very well suited for edge poloidal current drive in RFPs. The strong poloidal upshift of the parallel wave number gives very strong electron Landau damping that localizes the narrow current profile to the edge region. We thus concur with Uchimoto who stated “the lower-hybrid (LH) slow wave is ideally suited for poloidal current drive in the outer region of the RFP” [1]. The simulations also indicate that the interdigital line should perform well as a launch structure for a slow wave with appropriate parallel wave number. The interdigital line also has good directivity, manageable ohmic losses and good plasma load in MST.

We have also shown that VORPAL<sup>®</sup> time-domain simulations can replace traditional RF coupling calculations if at least a medium-sized cluster is available. Finite-difference spatial discretization does an excellent job of modeling the most complicated launch structures when Dey-Mittra cut cells are used. This was demonstrated by a blind validation exercise where VORPAL computed the voltage phasing of the interdigital line within roughly one degree of the experimental value. In vacuum, the experimental and VORPAL values for the parallel refractive index are the same,  $n_{\parallel} = 6.8$ . With flattened antenna models, MWS computed an  $n_{\parallel} = 6.7$  (Chapter 3.1.3 of Ref. [8]) and COMSOL  $n_{\parallel} = 6.3$  [11]. The large error for the COMSOL results is not understood, but insufficient numerical resolution was ruled out [11]. An MWS simulation with the realistic, curved antenna was performed, but the result was worse than for the flattened antenna, possibly due to the need for higher numerical resolution to resolve the curved geometry.

It should be mentioned that the relatively small computational-domain size for the VORPAL simulations presented here should be sufficient when there is no cut off inside the plasma, i.e. when the parallel wave number is large enough. However, if there is a cut off inside the plasma, but outside of the computational domain, the PML boundary will nonphysically absorb the wave energy before it is reflected against the cut-off layer. If this numerical damping is more or less matched by Landau damping in the real world, the simulations results should still be valid. However, if the numerical damping is much stronger than the real Landau damping, the simulations could be overly optimistic about the antenna performance. This might have affected our simulations of the existing MkIII version of the antenna (Case A above). For future work, care should be taken to make sure the computational domain is large enough to include any cut-off layer.

The experimental results for the MST interdigital line MkIII antenna are inconclusive. This is to be expected, given that the RF power used was at least an order of magnitude below the 1 MW estimate given by Uchimoto for significant current drive. There might also be an accessibility problem due to the too-low parallel wave number of the launched wave. This would be consistent with experimental observations of hard x-ray emission (above 10 keV) at the plasma edge, believed to be caused by bremsstrahlung from a population of fast, ponderomotively accelerated electrons (see Chapter 4.3 of Ref. [8] for details). Poor accessibility, with resultant reflection against

the cut-off layer, will build up the field amplitude and open various channels of parasitic absorption. Another indication of poor accessibility in the experiment is that ohmic heating and through power (Poynting flux reaching the output feed) is several times larger than in the simulations (see Chapter 2.7 of Ref. [8]). This could be explained by radiated power being reflected back into the launch structure. Shifting the focus of the VORPAL/RANT3D simulations from the antenna to the wave propagation and absorption in the plasma could help shed light on the performance of the MkIII antenna.

The VORPAL simulations presented here do an excellent job of modeling antenna performance and wave propagation in the plasma. They do not capture electron Landau damping, the dominant absorption mechanism. To extend the simulations to incorporate Landau damping by using kinetic electrons at the relatively low frequency of 800 MHz would take us to the leading edge of supercomputing. A much more sensible approach would be to leave the absorption computation for RANT3D/AORSA1D-H, which does an excellent job for propagation/absorption if given a correct antenna current distribution as input. The combination of VORPAL, or a code with similar capabilities, together with the efficient and reliable workhorse RANT3D, is something that is worth consideration for RF coupling simulations in general.

## Acknowledgments

This work was funded by ORNL contract #4000047802 and DOE grant #DE-FG02-09ER55006. Thanks to Drs. D. Rasmussen and J. Caughman at ORNL for their support for this work, Dr. M. Carter (ORNL) for helping us get proficient with RANT3D/AORSA1D-H and Dr. J. Anderson (UW) for the MST equilibrium data. Thanks to Dale Schutte, Andrey Levochkin and Paul Wilhite at UW for providing the necessary computational resources and outstanding technical support.

- [1] Uchimoto E, Cekic M, Harvey R W, Litwin C, Prager S C, Sarff J S and Sovinec C R 1994 *Physics of Plasmas* **1** 3517–3519
- [2] Dexter R, Kerst D, Lovell T, Prager S and Sprott J 1991 *Fusion Technology* **19** 131
- [3] Goetz J, Thomas M, Forest C, Prager S, Uchimoto E, Baity F and Pinsker R 2001 *AIP Conference Proceedings* vol 595 p 253
- [4] Matthaei G L 1962 *IRE Transactions on Microwave Theory and Techniques* **10** 479–491
- [5] Moeller C, Gould R, Phelps D and Pinsker R 1994 *AIP Conference Proceedings* vol 289 p 323
- [6] Takase Y, Ejiri A, Kasuya N, Mashiko T, Shiraiwa S, Tozawa L, Akiduki T, Kasahara H, Nagashima Y, Nozato H, Wada H, Yamada H, Yamada T and Yamagishi K 2001 *Nuclear Fusion* **41** 1543
- [7] Takase Y, Moeller C, Seki T, Takeuchi N, Watari T, Callis R, Ejiri A, Ikezi H, Kasahara H, Kasuya N *et al.* 2004 *Nuclear Fusion* **44** 296
- [8] Kaufman M C 2009 *Lower Hybrid Experiments Using an Interdigital Line Antenna on the Reversed Field Pinch* Ph.D. thesis University of Wisconsin-Madison
- [9] Carter M, Rasmussen D, Ryan P, Hanson G, Stallings D, Batchelor D, Bigelow T, England A, Hoffman D, Murakami M *et al.* 1996 *Nuclear Fusion* **36** 209
- [10] Nieter C and Cary J R 2004 *Journal of Computational Physics* **196** 448–473
- [11] Shiraiwa S, Meneghini O, Parker R, Bonoli P, Garrett M, Kaufman M C, Wright J C and Wukitch S 2010 *Physics of Plasmas* **17** 056119
- [12] Golant V E 1972 *Soviet Physics – Technical Physics* **16** 1980–1988

- [13] Smithe D N 2007 *Physics of Plasmas* **14** 056104
- [14] Berenger J P 1994 *Journal of Computational Physics* **114** 185–200
- [15] Dey S and Mittra R 1997 *Microwave and Guided Wave Letters, IEEE* **7** 273–275
- [16] Carlsson J, Smithe D, Carter M and Kaufman M 2008 *Bulletin of the American Physical Society* **53** 58

This is an author-created, un-copyedited version of an article accepted for publication in Plasma Physics and Controlled Fusion. The publisher is not responsible for any errors or omissions in this version of the manuscript or any version derived from it. The Version of Record is available online at <http://dx.doi.org/10.1088/0741-3335/56/5/055007> .